Braz J Phys (2015) 45:195–199
DOI 10.1007/s13538-015-0305-3

ATOMIC PHYSICS

A Simple Model for Ice Compaction Data Induced by Low Energy Ion Irradiation

A. L. F. de Barros · C. Mejía · W. A. M. Morgado · L. F. Almeida · E. F. da Silveira

Received: 13 December 2014 / Published online: 5 February 2015

Abstract A connection between the compaction of amorphous solid water (ASW) during energetic ion irradiation and the disappearing of water dangling bonds (OH-db) has been analyzed particularly by the Palumbo et al. and by Baragiola et al. In this work, a further discussion of the process for inducing the compaction is presented. Simple models for OH-db evolution for irradiated water ice are discussed. Literature results on the OH-db disappearance in ices bombarded by 100–200 keV H^+ ions and on the comparison of porosity and OH-db results for 200 keV Ar^+ ions are revisited. It is observed that for both, porosity decrease (compaction) and OH-db absorption signal decrease, experimental data can be well fitted by the sum of two decreasing exponentials with similar sets of parameters. Although a clear explanation for this correlation cannot be extracted, it suggests strongly that compaction and OH-db destruction are both triggered by two different processes.

Keywords Cosmic rays · Molecules ionization · Modeling data

1 Introduction

In the interstellar medium (ISM), where temperatures can be as low as 10 K, most of the gases are condensed in grains or on surfaces of solid bodies. In this environment, ices are processed by cosmic ray ions and by UV photons. Fast ions passing through solid transfer energy to the target material at a rate defined as stopping power. Atomic cascades [1] and electronic excitation [2, 3] take place and, as a consequence, many molecular bonds are typically broken along the ion track generating rearrangement of the lattice structure and allowing molecular fragments to recombine into new chemical species. In order to understand the cosmic ray interaction with ices, experiments have been performed in laboratories to take advantages of analytical techniques such as Rutherford Backscattering—RBS [e.g., [4]], infrared spectroscopy—FTIR [5–9], interferometry [10], and mass spectrometry—MS [11, 12]. In particular, phase transitions in water ice occur when the ice is irradiated at low temperature (T<120 K) with fast ions [12–14]. The use of OH-dangling bond infrared absorption to probe water ice cluster surfaces and within pores of amorphous ice was employed in the early 1990s [6, 15].

Nevertheless, relevant characteristics of ice compaction have been established by many authors [e.g., 16–19]; the process is not yet fully understood. It is expected that the energy deposited by energetic projectiles induces molecular motion that alters the ice structure and minimizes the internal surface energy via the collapse of void structures (e.g., micro-pores) of the target. Compaction should therefore depend on the ion-ice stopping power. Another relevant aspect is the structure of the pores: are they spherical (like bubbles), laminar (spaces between close walls), or filamentary. Are they separated or interconnected?

The main goals of the current article are the following:

(i) Pursue the analysis on the connection between ice porosity and IR absorbance by OH-dangling bonds
(ii) Contribute for the understanding of the compaction process by ion irradiation

The current analysis discusses published FTIR results concerning the OH-db signals from ices bombarded by 100–

A. L. F. de Barros (✉) · L. F. Almeida
Departamento de Física, Centro Federal de Educação Tecnológica Celso Suckow da Fonseca -CEFET/RJ, Av. Maracanã 229, Rio de Janeiro, RJ 20271-110, Brazil
e-mail: abarros@pq.cnpq.br

C. Mejía · W. A. M. Morgado · E. F. da Silveira
Departamento de Física, Pontifícia Universidade Católica do Rio de Janeiro, Rua Marquês de São Vicente 225, Rio de Janeiro, RJ 22453-900, Brazil

200 keV H^+ ions [16]. They are compared with also published results on porosity and OH-db obtained for 200 keV Ar^+ ions [17].

2 Modeling the Evolution of the OH-db Population and of the Ice Porosity

2.1 The OH-db Population on Target Surface

The model considers that the OH-dangling bonds exist only for water molecules adsorbed on the ice surface with an areal density n_S. The OH-db are destroyed when the flat ice surface is bombarded perpendicularly by fast projectiles with flux Φ (projectiles per area and time units); after a time interval Δt, the beam fluence is $\varphi=\Phi\,\Delta t$.

The OH bonds are broken if they are inside a circle of radius r_S centered in the impact point; the decreasing rate $dn_S/d\varphi$ should depend on both r_S and n_S; n_S is expected to be a decreasing function of φ but may not vanish if new bonds are created by the beam. Two extreme cases are easier to be modeled: n_S is very low (the average distance between two bonds is much greater than r_S and one bond at most is destroyed per impact) or n_S is very high (the average distance between two bonds is much smaller than r_S).

If formation of OH-db is neglected, the number dn_S of bonds destroyed per area unit during the time dt is as follows:

$$dn_S = -n_S \pi r_S^2 \Phi dt = -n_S \sigma_S d\varphi, \tag{1}$$

where $\sigma_S=\pi r_S^2$. The integration of this expression is straightforward:

$$n_S = n_{S0}\ \exp(-\sigma_S \varphi). \tag{2}$$

If Y_{db} OH-dangling bonds are produced per impact, then $dn_S=(-n_S\sigma_S+Y_{db})d\varphi$ and the normalized column density of OH-db writes:

$$\frac{n_S}{n_{S0}} = \frac{Y_{db}}{n_{S0}\sigma_S} + \left(1-\frac{Y_{db}}{n_{S0}\sigma_S}\right)\ \exp(-\sigma_S\varphi). \tag{3}$$

In the low regime fluence, $\sigma_S\,\phi<<1$, one has approximately:

$$\frac{n_S}{n_{S0}} = 1-\left(\sigma_S-\frac{Y_{db}}{n_{S0}}\right)\ \varphi. \tag{4}$$

2.2 The Pore Population in the Target Bulk

In general, ice films produced by vapor deposition do not have a crystalline structure since their molecules are disoriented and disordered. Voids also exist in the bulk, characterizing a porosity P defined by $P=1-\rho/\rho_c$, where ρ is the average film density of the amorphous sample and ρ_c is the density crystalline structure [18]. Mass densities can be determined directly via mass (quartz crystal microbalance) and thickness (light interferometry) measurements. For compact amorphous water ice, $\rho_c=0.94$ g/cm^3 [19].

Pore collapse occurs when the ice is irradiated: from the initial porosity, P_0, to the final porosity $P(\varphi)$ as decreases continuously with the beam fluence, ϕ. A convenient procedure for comparing porosity and OH-db results is to define the normalized porosity by the ratio $P(\varphi)/P_0$.

A porous ice film of thickness h is considered; inside the ice, identical spherical pores of radius R_p are distributed uniformly with density n_p/h, where n_p is the column density of pores (Fig. 1). The film is thin enough to be traversed by projectiles with approximately constant velocity. It is assumed that each projectile generates a cylinder of radius b, co-axial with its trajectory inside, which all pores are destroyed.

Similarly, to the development presented in the previous section, the number of destroyed pores by $d\varphi$ projectiles per area unit is:

$$dn_P = -n_P \sigma_P d\varphi, \tag{5}$$

where $\sigma_p=\pi b^2$.

Alternative conditions may be taken into account for the pore collapse, as for instance, the contact between pore and the projectile track; in this case, $\sigma_p=\pi\ (b+R_p)^2$. The number of surviving pores as a function of fluence is predicted to be:

$$n_p = n_{p0}\ \exp(-\sigma_p\varphi). \tag{6}$$

Formation of pores by irradiation may also occur if molecules of a very low sublimating temperature are dispersed on the water ice; in the temperature rising after the projectile passage, these molecules have enough mobility to form bubbles.

2.3 The OH-db Population on the Pore Surface

Assuming that each pore contains k OH-db bonds and that all of them are quenched when the pore collapses, the column density of surviving bonds in the bulk is $n_b=k\,n_p$. The evolution of pore population is described by:

$$n_B = n_{B0}\exp(-\sigma_p\varphi). \tag{7}$$

More realist spherical approaches can be taken to account an R_p—distribution for which the parameter k varies with R^2. If other pore shapes are considered, k will depend on the corresponding variables. More complex models are necessary if the pores are interconnected: the projectile melts and/or sublimates the ice around its track, causing high-pressure fluid injection into the neighboring pores or micro-caves. The flooded region is determined by the fluid re-solidification.

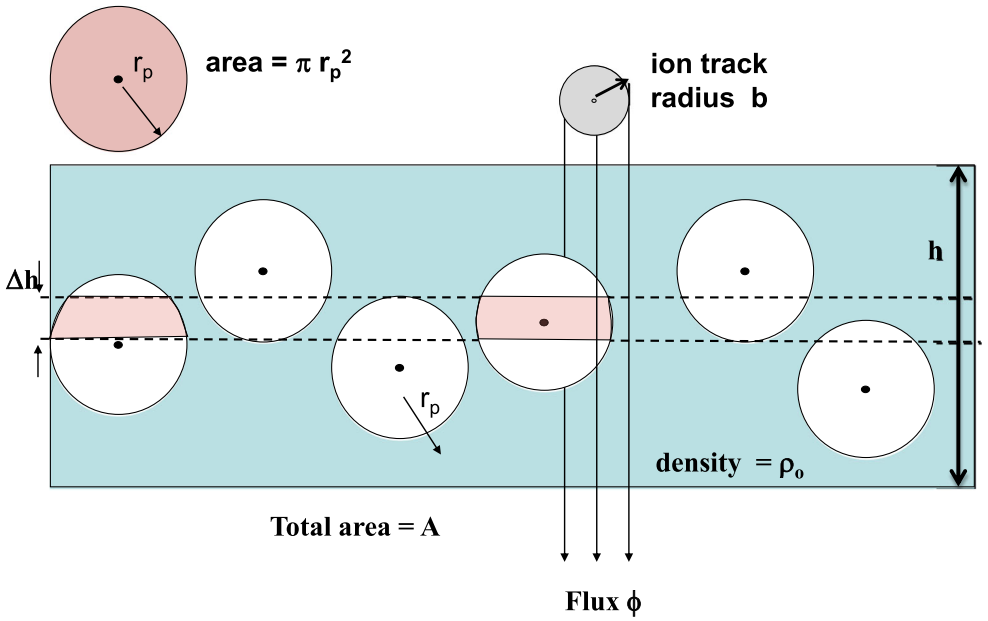

Fig. 1 Sketch of an ice film with spherical pores traversed by fast atomic ions

The pore interconnection is progressively blocked, the percolation ceases, and the compaction process becomes less efficient for higher fluence. Such analyses are however beyond the scope of this work.

2.4 The OH-db Population on the Surface and in the Bulk of the ice

The OH-dangling bonds are usually formed on the ice surface during its grown by the vapor deposition. Their column density n_S should depend on the deposition rate and the ice temperature. In a certain extent, the surface roughness of the ice film may be considered as constituted by open or unfinished pore structures; on the other hand, for experiments using ion beams, such open pores in the surface are always in vacuum, cannot be flooded, and their OH-db are destroyed not in the same way as bulk ones are. The processes described by Eqs. (2) and (7) may occur independently and the total OH-db column density decreased rate is the sum of the corresponding rates: $dn/d\varphi = dn_s/d\varphi + dn_b/d\varphi$. Integrating the expression, one gets:

$$n(\varphi) = \left(n_{S0} - \frac{Y_{\mathrm{db}}}{\sigma_S}\right) \exp(-\sigma_b\varphi) + n_{B0}\exp(-\sigma_b\varphi) + n(\infty) \tag{8}$$

The OH-db destruction cross-section in the bulk, σ_b, may not be the same as the pore destruction σ_p. For instance, a weak annealing may destroy the OH-db but not the all the pores. Anyhow, a double-exponential decrease with an off-term level is qualitatively predicted.

3 Data Analysis

3.1 OH-db Measurements

Palumbo et al. [16] and Raut et al. [17] have analyzed FTIR spectra of ASW taken after irradiation at different fluences with 200 keV H^+ and 100 keV Ar^+ ions, respectively. Palumbo fitted the H^+ data with Eq. (7) and found $\sigma_p = 4.13\times10^{-14}$ cm^2. The fitting of the Ar^+ data with a single exponential plus a constant gives $\sigma_p = 10\times10^{-14}$ cm^2. Both fittings of the normalized OH-db signals are displayed in dotted lines in Fig. 2. For clarity sake, two different scales are employed: log-log scale in Fig. 2a and semi-log in Fig. 2b. The dash and solid lines represent fittings by the sum of two exponentials, corresponding to Eq. (8) with $n(\infty)=0$. The obtained parameters are presented in Table 1 ($\sigma = 2\pi r^2$).

The following observations can be extracted from inspection of Fig. 2:

(i) The 100 keV Ar^+ ions are much more efficient than 200 keV H^+ ions for destroying OH-db. The corresponding cross-sections of Ar^+ are about thre times larger than the H^+ ones.

(ii) For each projectile species, the db band area decrease is not described correctly by a single exponential (or an exponential plus a constant) but rather by the sum of two of them. Particularly from inspection of line shapes in Fig. 2b, two regimes seem to occur, one at low and the other at high beam fluence.

(iii) The order of magnitude of the ratio σ_1/σ_2 is about the same (~10) for both projectile species; as a consequence, one curve can be transformed into the other by re-scaling the fluence axis. In effect, the dash line

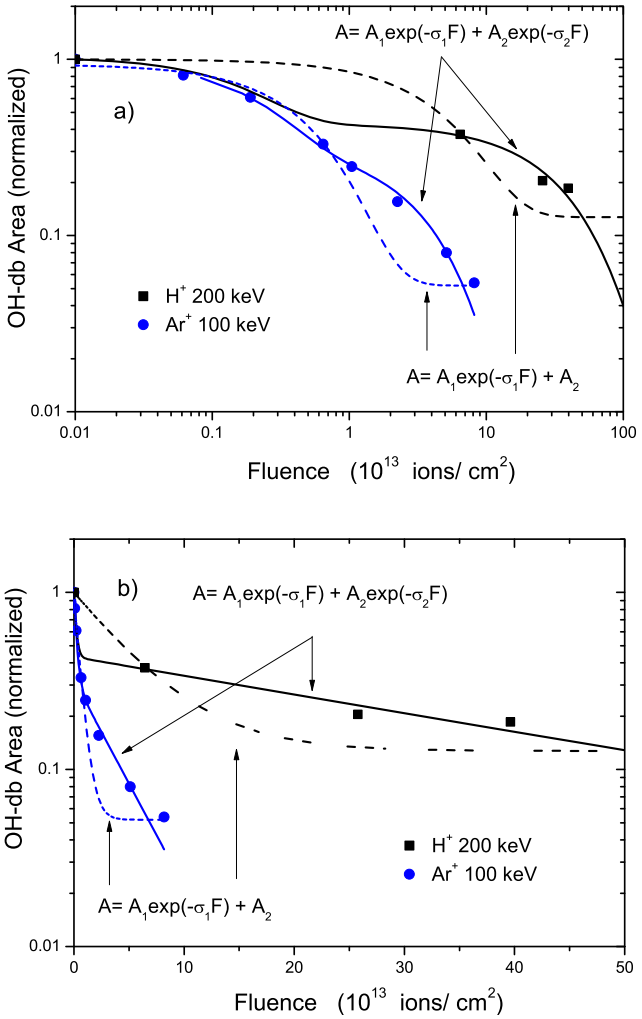

Fig. 2 Decrease of the OH-db signal when a pure water ice is bombarded by H^+ [16] and by Ar^+ [17] projectiles. Curve with dots: fitting by an exponential plus a constant; dash lines: Ar^+ data fitted by a sum of two exponentials; solid line: H^+ data fitted by a sum of two exponentials. **a** log-log display; **b** log-linear display

obtained by multiplying the Ar^+ fluence values by the factor 3.3 fits the H^+ data as well. Note that this operation is equivalent of saying that σ_1 (Ar^+)/σ_1 (H^+)=σ_2 (Ar^+)/σ_2 (H^+)=3.3. The quality of the transformation can be estimated in Fig. 3, where the same experimental data is displayed and compared with calculations.

3.2 Porosity Measurements

For amorphous solid water bombarded with 100 keV Ar^+ ions, the decrease of porosity and the OH-db destruction have been measured and compared to each other by Raut et al. [18]. Their results, the normalized functions $P(\varphi)/P_0$ and $n(\varphi)$/n(0), are displayed in Fig. 3a, and the fitting parameters are presented in Table 1.

The similarity between the two curves is obvious. The porosity decrease is well fitted by the double-exponential function, but the pore destruction process is slower than the OH-db destruction. The σ_p cross-section values are consequently lower than the σ_b ones. It is worthy of note that the ratio $\sigma_1/\sigma_2 \sim 10$ is about the same for the OH-db and for the pore destruction. Again, the re-scaling the fluence axis by a factor 6 brings the overlapping of the two curves (dashed line), as also shown in Fig. 3b. Baragiola et al. proposed that during irradiation, coalescence of pores or smoothing of walls occurs causing reduction of the total surface area faster than the pore volume [14].

4 Conclusion

A simple model predicts a double-exponential decay for the OH-db signals when an amorphous water ice is bombarded by fast ions. The FTIR results of two measurements found in the literature were revisited, and we found that data are compatible with the predicted double-exponential dependence on the beam fluence. It is expected that the origin of the two exponentials would come from different locations of OH-db, such as target surface and pore surface positions or from different destruction processes of the bonds, such melting, shock waves, or dissociation by secondary electron interaction or atomic cascade released by the interaction of water molecules with the ion in the track. These secondary phenomena can deliver energy to the OH-db dissociation or rearranging in the ice surface.

Porosity measurements are particularly helpful in the discussion of the OH-db phenomenon since the pore collapse reflects a bulk characteristic (ice compaction) but may not interfere with OH-db at the target surface. Interestingly, experimental data show a close connection between porosity

Table 1 Cross-sections (in 10^{-14} cm^2) for ice water obtained for the double-exponential fitting for H^+ and Ar^+ beams. The two first lines correspond to FTIR experiments in which the OH-db signals were analyzed. The third line corresponds to porosity measurement

Projectile	E (keV)	Experim.	σ_1 (10^{-14} cm^2)	r_1 (Å)	σ_2 (10^{-14} cm^2)	r_2 (Å)	σ_1/σ_2	Ref
Ar^+	100	OH-db	33	18	2.5	5.0	13	[18]
H^+	200	OH-db	10	10	1.0	3.2	10	[17]
Ar	100	porosity	6.3	8.0	.55	2.4	11	[18]

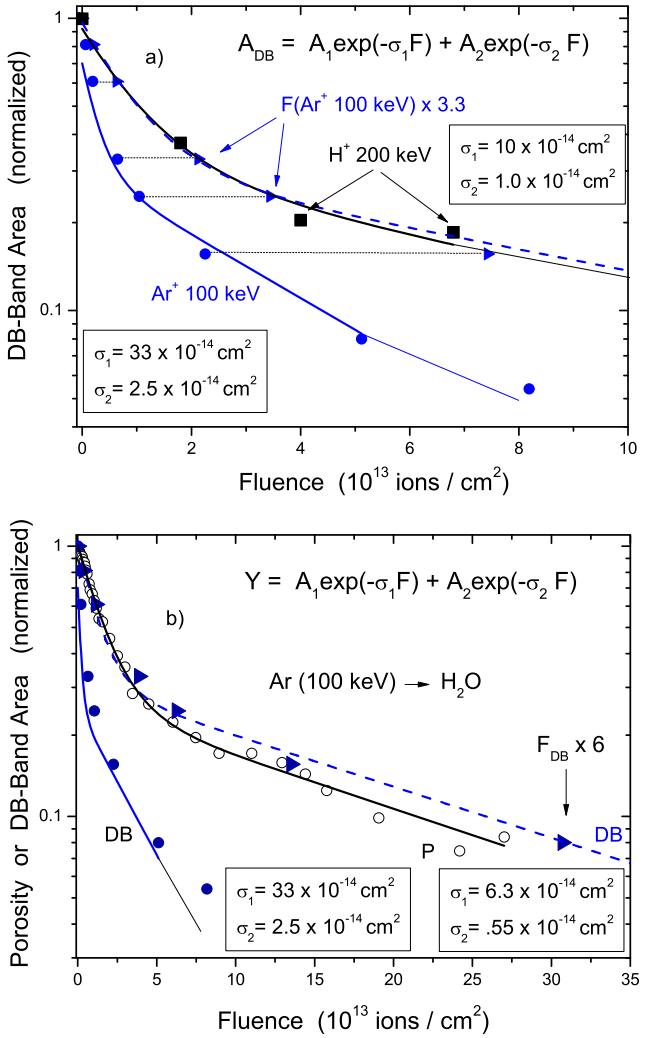

Fig. 3 In **a** OH-db band area dependence on beam fluence for 200 keV H^+ (black squares) and for 100 keV Ar^+ ions (blue circles). Both exponential components for the Ar^+ fitting are shown. The dot line is the fitting and the dash line is the Ar^+ data re-scaled in fluence by a factor 3.3. Data from [16, 17]. In **b** Normalized porosity and OH-db band area dependence on beam fluence for 100 keVAr^+ ions. The dash lines is the OH-db Ar^+ data re-scaled in fluence by a factor 6. Data from [17]. All the curves are normalized to unit at $\varphi=0$. The curves are fittings using Eq. (8) without the constant term

variation and OH-db destruction: they are not proportional to each other but both decrease as a double-exponential function with correlated parameters. It is difficult to give a secure explanation based only on the discussed data; however, they seem to be consistent enough to motivate more experiments with this goal.

Acknowledgments The authors thank the Brazilian foundations CNPq (INEspaço), FAPERJ and CAPES for the financial support.

References

1. G. Falcone, Riv Nuovo Cimento **13**, 1 (1990)
2. B.U.R. Sundqvist, A. Per Håkansson, D. Hedin, G. Fenyö, P. Brinkmalm, Roepstorff, R.E. Johnson, in *Methods and Mechanisms for producing Ions from Large Molecules*, ed. by K.G. Standing, W. Ens (Plenum Press, New York, 1991)
3. W.L. Brown, W.M. Augustyniak, K.J. Marcantonio, E.H. Simmons, J.W. Boring, R.E. Johnson, C.T. Reimann, Nucl. Inst. Methods Phys. Res. B **1**, 307–314 (1984)
4. W.L. Brown, L.J. Lanzerotti, J.M. Poate, W.M. Augustyniak, Phys. Rev. Lett. **40**, 1027 (1978). RBS
5. W. Hagen, A.G.G.M. Tielens, J.M. Greenberg, A&A **117**, 132 (1983)
6. B. Rowland, J.P. Devlin, J. Chem. Phys. **94**, 812 (1991)
7. G. Leto, G.A. Baratta, Astron Astrophys **397**, 7 (2003)
8. A.L.F. de Barros, A. Domaracka, D.P.P. Andrade, P. Boduch, H. Rothard, E.F. da Silveira, Mon. Not. R. Astron. Soc **418**, 1363 (2011)
9. C. Mejia, A.L.F. de Barros, E.D. Seperuelo, E.F. da Silveira, E. Dartois, A. Domaracka, P. Boduch, H. Rothard, Icarus **250**, 222–229 (2015)
10. J.B. Bossa, K. Isokoski, M.S. de Valois, H. Linnartz, A&A **545**, A82 (2012)
11. V.M. Collado, L.S. Farenzena, C.R. Ponciano, E.F. da Silveira, K. Wien, Surf. Sci. **569**, 149 (2004)
12. A.L.F. de Barros, L.S. Farenzena, D.P.P. Andrade, E.F. da Silveira, K. Wien, J. Phys. Chem. **115**, 12005 (2011)
13. R. Matthäus, R. Moshammer, PDMS and clusters, in *Lecture Notes in Physics*, ed. by E.R. Hilf, F. Kammer, K. Wien, vol. 269 (Springer, Berlin, 1986), p. 241
14. R.A. Baragiola, M. Famá, M.L. Loeffler, U. Raut, J. Shi, Nucl. Instrum. Meth. Phys. Res. B **266**, 3057 (2008)
15. B. Rowland, M. Fisher, J.P. Devlin, J. Chem. Phys. **95**, 1378 (1991)
16. M.E. Palumbo, Astron. Astrophys. **453**, 903 (2006)
17. U. Raut, B.D. Teolis, M.J. Loeffler, R.A. Vidal, M. Famá, R.A. Baragiola, J. Chem. Phys **126**, 244511 (2007)
18. U. Raut, M. Famá, M.J. Loeffler, R.A. Baragiola, Astrophys. J. **687**, 1070 (2008)
19. A.H. Narten, C.G. Venkatesh, S.A. Rice, J. Chem. Phys. **64**, 1106 (1976)